Wind and Structures, Vol. 16, No. 3 (2013) 225-240
DOI: http://dx.doi.org/10.12989/was.2013.16.3.225

Wind tunnel studies of cantilever traffic signal structures

Héctor J. Cruzado*[1], Chris Letchford[2] and Gregory A. Kopp[3]

[1]Department of Civil and Environmental Engineering, Polytechnic University of Puerto Rico, San Juan, USA
[2] Department of Civil and Environmental Engineering, Rensselaer Polytechnic Institute, Troy, NY, USA
[3]Boundary Layer Wind Tunnel Laboratory, Faculty of Engineering, University of Western Ontario
London, Ontario, Canada

(Received May 12, 2011, Revised July 27, 2011, Accepted January 29, 2012)

Abstract. The wind-induced vibrations of the mast arm of cantilever traffic signal structures can lead to the fatigue failure of these structures. Wind tunnel tests were conducted on an aeroelastic model of this type of structure. Results of these experiments indicated that when the signals have backplates, vortex shedding causes large-amplitude vibrations that could lead to fatigue failure. Vibrations caused by galloping were only observed for one particular angle of attack with the signals having backplates. No evidence for galloping, previously thought to be the dominant cause of fatigue failures in these structures, was observed.

Keywords: cantilevered traffic signal structures; fatigue; wind-induced vibrations; galloping; vortex shedding

1. Introduction

Large amplitude vibrations of mast arms of cantilever traffic signal structures can occur at wind speeds as low as 4.5 m/s (Pulipaka, Sarkar and McDonald 1998). If the vibrations are too large, they could make it difficult for drivers to see the signals or could create concern about driving under the vibrating structure (Kaczinski, Dexter and Van Dien 1998). More importantly, the vibrations can lead to the fatigue failure of the mast arms. In the United States, several state transportation departments have reported such fatigue failures. Many of the failures are caught before there is a collapse. Still, a few collapses are reported each year and, in some cases, vehicles have collided with a fallen mast arm causing serious injuries and deaths (Dexter and Ricker 2002).

Conducting water-table, tow-tank, wind tunnel, and field experiments, Pulipaka (1995) determined that large amplitude vibrations occur when the wind blows from the backside of the signal lights having backplates. He concluded that these large amplitude vibrations are due to the galloping phenomenon.

There are four recognized mechanisms that induce mast arm vibrations on cantilever traffic signal structures: galloping, natural wind gusts, truck-induced gusts, and vortex shedding. Probably because of the research by Pulipaka (1995) and Pulipaka, Sarkar, and McDonald (1998), it has generally been thought that galloping is the main cause of vibrations that lead to fatigue failure of mast arms, that natural wind gusts and truck-induced gusts are minor causes, and that

*Corresponding author, Professor, E-mail: hcruzado@pupr.edu

vortex shedding does not cause significant vibrations. This has been so widely accepted in the United States that the national design guidelines do not consider vortex shedding in the fatigue design of cantilever traffic signal structures (AASHTO 2001). Further investigations on the vibrations of cantilevered traffic signal structures have been mostly concentrated on implementing damping devices (Cook *et al*. 2001, McManus *et al*. 2003, Christenson and Hoque 2011) or on increasing the fatigue resistance (Puckett *et al*. 2010, Park *et al*. 2011). These investigations have been conducted either, under the assumption that galloping is the major cause of fatigue failure or without taking into consideration of which is the vibration-inducing mechanism.

Research was conducted at Texas Tech University (TTU) on full-scale cantilever traffic signal structures (Cruzado 2007, Zuo and Letchford 2010). Their findings contradict previous studies by indicating that vortex shedding could in fact be a major cause of large amplitude vibrations that could lead to the fatigue failure of mast arms. To complement the full-scale experiments conducted at TTU, wind tunnel experiments were conducted using aeroelastic models of cantilever traffic signal structures. The wind tunnel tests were initially conducted at the Boundary Layer Wind Tunnel Laboratory of the University of Western Ontario (UWO) and were later continued at TTU's Boundary Layer Wind Tunnel.

For the present work, the objectives were to determine the mechanisms that lead to mast arm vibrations and their significance in contributing to the fatigue failure of these structures. Full-scale experiments and wind tunnel tests were conducted in order to achieve this objective; however, only the wind tunnel tests are discussed in this paper. The full-scale experiments are discussed in an accompanying paper.

2. Wind tunnel experiments

2.1 University of Western Ontario experiments

2.1.1 Model design and construction

Traffic signal structures come in many different sizes and shapes. It was decided that the model should specifically replicate the cantilever traffic signal structure with a 13.4-m mast arm used in full-scale measurements by TTU because this structure had been seen vibrating significantly in the field experiments (Cruzado 2007). Fig. 1 shows the dimensions of the structure and of the signal light heads it supports.

It was also decided that the model would be tested in the small, open circuit, Aerodynamics Wind Tunnel (AWT) at UWO, which has a 46-cm x 46-cm section. Because of the length scale selected (1:50) and the fact that the mast arm stiffness was much lower than the pole, it was decided to model only the mast arm, eliminating the pole. Furthermore, most failures have been documented at the pole-mast junction (Pulipaka 1995, Gray *et al*. 1999, Hartnagel and Barker 1999, Hamilton *et al*. 2000, Chen *et al*. 2001, Cook *et al*. 2001).

With the pole eliminated, the mast arm model was mounted vertically and tested in uniform flow, which approximates the full-scale conditions; the mast arm cantilevers horizontally and does not see a velocity gradient along its length. Also, by placing the mast arm vertically, the effects of gravitational loads were neglected because they were expected to play little role in aerodynamic behavior. Since gravity loads had already been neglected by placing the mast arm model vertically, Froude scaling was not required and a velocity scale of λ_U = 1/1 was selected. Therefore with a length scale of λ_L =1/50, the elastic stiffness scale (λ_{EI}) was obtained as:

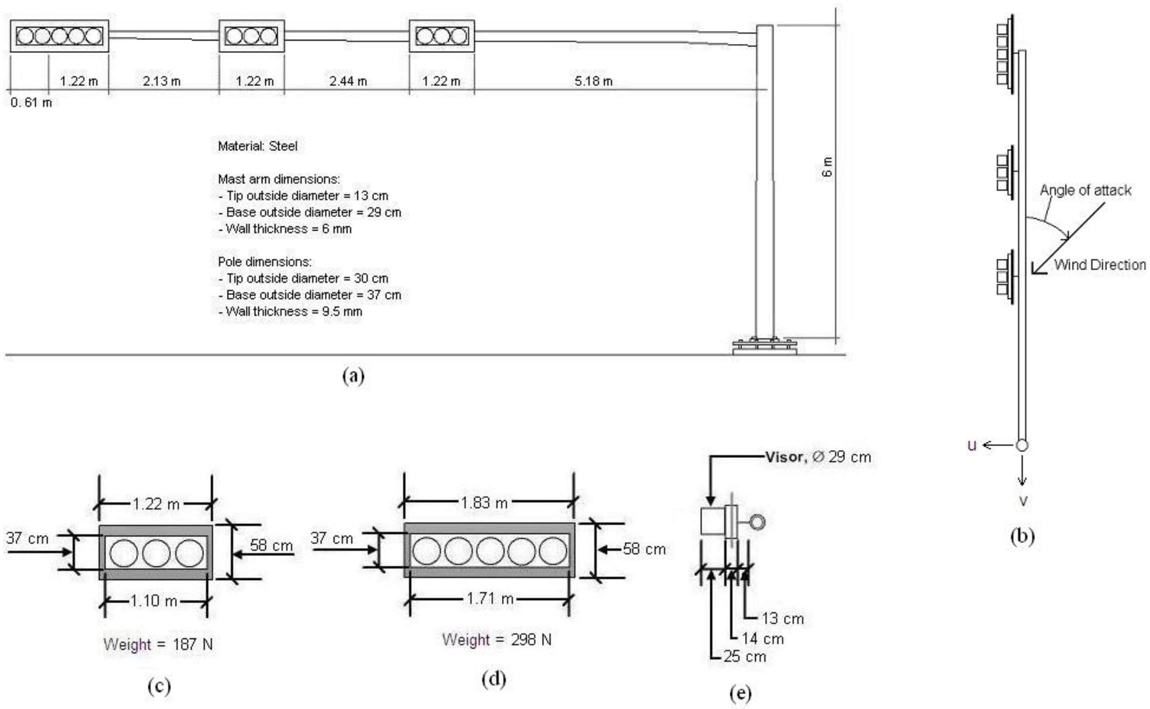

Fig. 1 (a)Geometry and light configuration of traffic signal structure with 13.4-m mast arm, (b) Angle of attack convention; Dimensions of signal light heads (shown with backplates), (c) 3-lights head, (d) 5-light head and (e) side view of 3- and 5-light heads

$$\lambda_{EI} = \lambda_U^2 \, \lambda_L^4 = (1/1)^2 \, (1/50)^4 = 1.6 \times 10^7 \tag{1}$$

To avoid high costs of fabrication, it was decided to use available sizes of aluminum or steel tubing to make the mast arm model. Since these are not available in tapered sections like the full-scale mast arm, the tapering was to be simulated by telescoping three different sizes of available tubing to form a single member. The length of each segment was established by arbitrarily deciding that the middle segment should carry the two 3-light signal heads. The mass, stiffness, and diameter that each segment required was determined using the corresponding scales (Cruzado 2007).

A design was determined in which the mast arm was to be made of aluminum with no cladding. The difficulty of this was finding available sizes of aluminum tubing with the required diameter, mass, and stiffness. Table 1 shows the best fit that was found. In the table, Segment 1 is connected to the fixed end, Segment 2 is in the middle supporting the two 3-light heads, and Segment 3 has the free end supporting the 5-light head. The table shows how the physical properties of the tubing (under the ‘Actual’ columns) match the required properties (as determined by the appropriate scales). It can be seen that greatest difficulty was found matching the elastic stiffness (*EI*). The scaled design is shown in Fig. 2, as well as the design of the light heads, which were made of foam, and attached to aluminum backplates.

It is known that

$$\lambda_f = \lambda_U \, / \, \lambda_L \tag{2}$$

Table 1 Comparison between the actual and required properties of the mast arm model

Segment	Diameter (mm)			Mass (g)			EI (kN-cm^2)		
	Required	Actual	% Diff.	Required	Actual	% Diff.	Required	Actual	% Diff.
1	5.21	5.56	-6.7	1.55	1.57	-1.3	13.12	14.44	-10.1
2	3.99	3.97	0.5	1.32	1.23	6.8	5.71	4.85	15.1
3	2.97	3.18	-7.1	0.54	0.53	1.9	2.30	2.32	-0.9

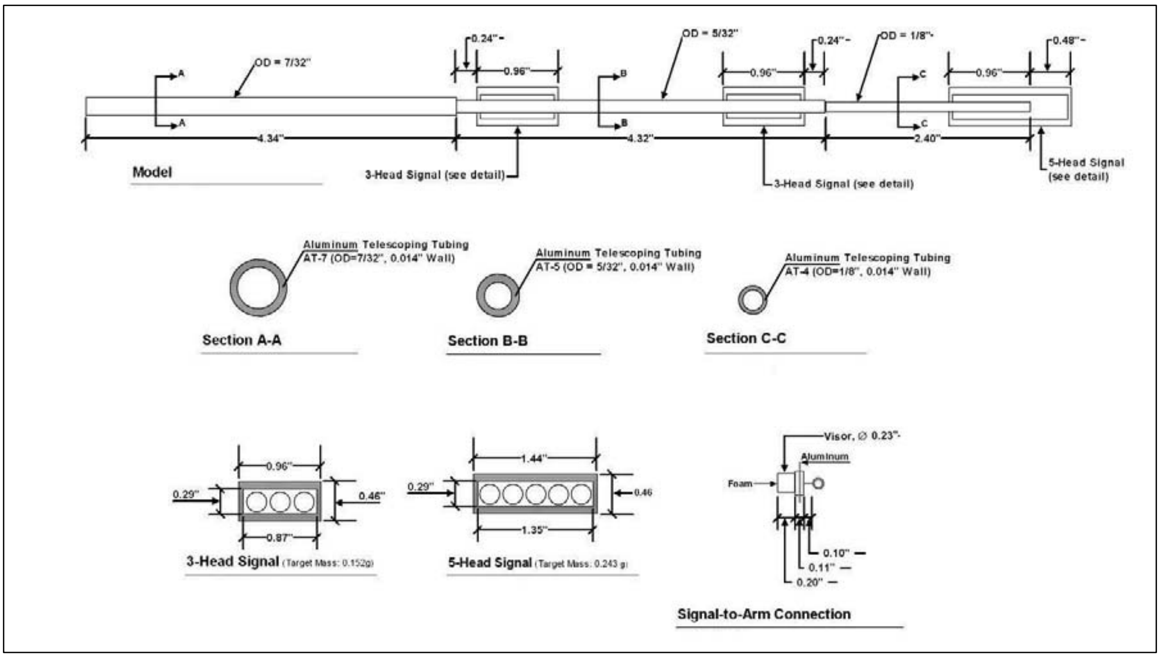

Fig. 2 Design drawing for the UWO wind tunnel model

where:

$\lambda_f = f_m / f_p$ = frequency scale

f_m = fundamental frequency of the model

f_p = fundamental frequency of the full-scale prototype

Therefore

$$f_m = f_p \lambda_U / \lambda_L \tag{3}$$

Since it is known that the in-plane fundamental frequency of the full-scale prototype is f_p = 0.98 Hz ≈ 1 Hz and that the model was designed with a length scale of λ_L = 1/50 and a velocity scale of λ_U = 1/1, then, substituting in Eq. (3), the expected fundamental frequency of the model was obtained

$$f_m = (1 \text{ Hz}) (1/1) / (1/50) = 50 \text{ Hz} \tag{4}$$

Once constructed, the model was attached to a JR3 load cell, which was connected to a data acquisition system. Exciting the tip of the model, the fundamental frequency of the model was determined from a Fast Fourier Transform (FFT) analysis of the load cell output. The model's fundamental frequency was measured as f_m = 62 Hz, which is 24% over the expected value. The authors believe that this large discrepancy is mostly due to the difference between the target and the actual stiffness's of the three segments. Accordingly the velocity scale was revised, while maintaining the elastic stiffness scale as before. This is not expected to cause any significant issues with the objectives of this work, which were to identify excitation mechanisms rather than to match an existing structure *per se*.

Solving Eq. (1) for the velocity ratio and substituting the actual values

$$\lambda_U = \lambda_f \lambda_L = (62/1)\,(1/50) = 1.24/1 \tag{5}$$

2.1.2 Experimental setup and procedure

The model was tested in the AWT at UWO. This wind tunnel has a maximum wind speed of 20 m/s. A Pitot-static tube was placed approximately 30 cm in front of the model and measured the wind speed. A Keyence LB-60 laser sensor with a range of 60 – 140 mm and a resolution of 40 μm (20 ms) – 180 μm (0.7 ms) was mounted in the plane of the model, as shown in Fig. 3, to measure the cross-wind displacements at the tip of the model. No along-wind measurements were made. All the data was collected at a sampling rate of 200 Hz (which translates to approximately 3.2 Hz in the full scale).

Two test configurations were studied under smooth uniform flow: with the signal orientated with the wind blowing onto the front, and then from the rear of the signals. Tests were conducted by sweeping wind speeds generally in an increasing manner and stopping at selected wind speeds where data was then recorded for statistically stationary periods of 2 minutes.

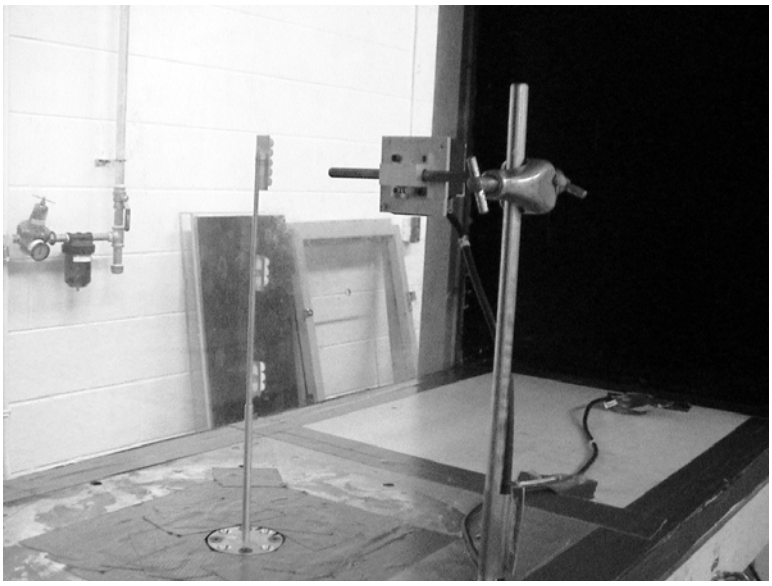

Fig. 3 Model and laser displacement monitor mounted in the AWT at UWO

2.1.3 Results

Significant cross-wind vibrations were observed when the model was tested with the wind blowing onto the back of the signals. These vibrations had a maximum peak-to-peak magnitude of approximately = 20 mm in the model scale. Since the model had a length of 281 mm, /L = 7.1%. These vibrations only occurred in a narrow wind speed range. No significant vibrations were observed when the model was tested with the wind blowing onto the front of the signals.

Fig. 4 shows concatenated time histories of the wind speed and of the cross-wind displacement of the tip when the model was tested with the wind blowing from behind the signals and with no grid installed in the tunnel. The time histories are not continuous as only the record of the stationary response is shown, once the desired wind speed was reached. Sometimes there could be an oscillation in approaching the desired wind speed, i.e., from above or below, and this could have led to some of the scatter in the observed peak response (Fig. 5). The figure values were scaled to full-scale using the length scale of 1/50, and the velocity scale of 1.24/1. It can be seen that large amplitude vibrations, sometimes having peak-to-peak amplitudes of 1 m, were observed when the wind speed was close to 5 m/s.

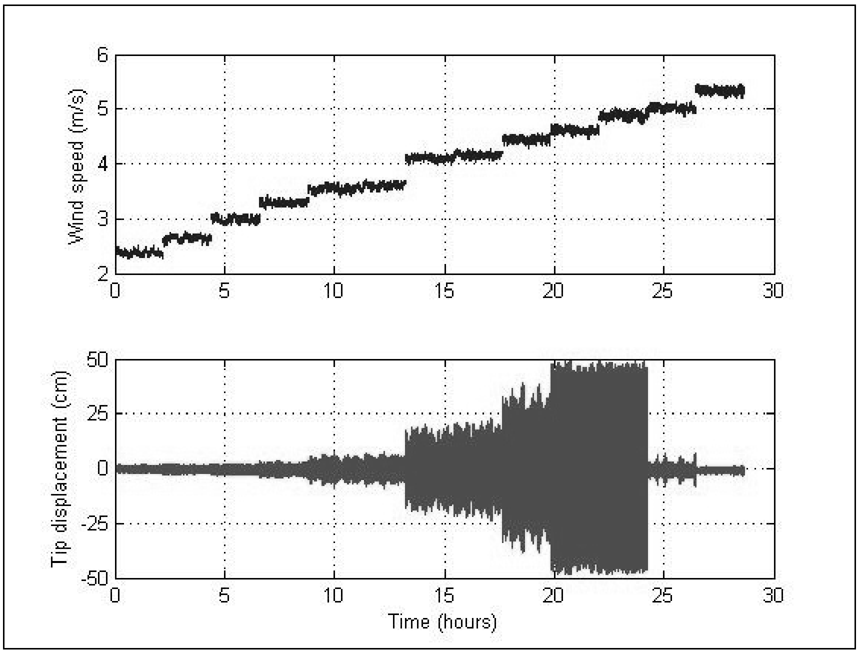

Fig. 4 Equivalent full-scale wind speed and displacement time histories for UWO wind tunnel tests

Average wind speeds (*U*) and standard deviations of the cross-wind displacement (*d*) were calculated using data segments of thirty-one (31) minutes in length from Fig. 4 (30 seconds in the model scale). Using the cross-wind width *B* (58-cm in full scale for the signal with backplates), an average non-dimensional tip displacement *d*/*B* was calculated. Also, using the vertical fundamental frequency f_0 = 1 Hz and the cross-wind width B, a reduced wind velocity of $U/(f_0 B)$ was calculated and then plotted versus the average non-dimensional tip displacement in Fig. 5. From this figure, it can be observed that the model exhibited a narrow band resonant response in the reduced wind speed range of 6 to 8. These resonant response at low speed is typical of a vortex shedding phenomenon causing the vibrations. The response shown in Fig. 5 remained unchanged for different averaging periods (for example, 124 minutes instead of 31 minutes).

2.2 Texas Tech University experiments

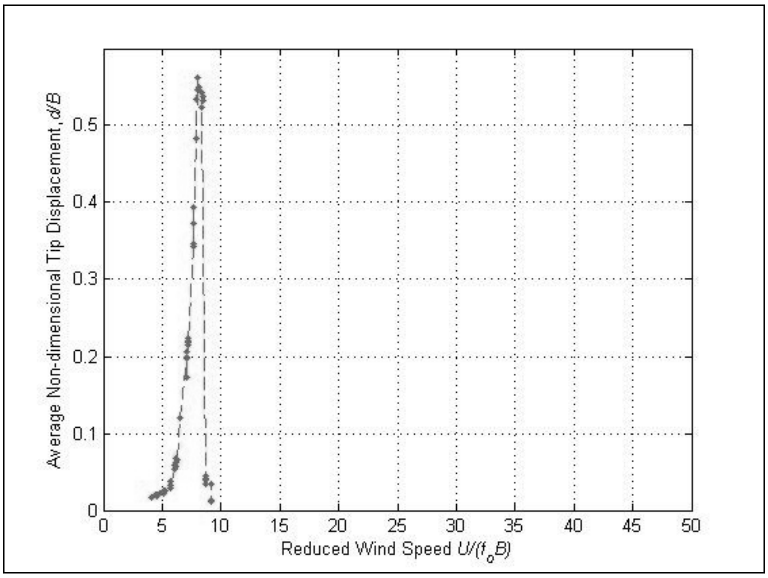

Fig. 5 Effect of wind speed on cross-wind displacement of tip for UWO wind tunnel tests

2.2.1 Model design and construction

For the TTU experiments, two models were used: (1) the same model of the mast arm with signals with backplates used at UWO, and (2) a new model identical to the previous one, excepting that the signals did not have backplates (i.e., the aluminum plate to which a signal is attached did not extend further than the foam simulating the signals). This way models could be tested with and without backplates.

2.2.2 Experimental setup and procedure

The mast arm model was clamped to a rigid pole (solid steel 19 mm diameter bar), which itself is attached to the turntable in the wind tunnel, as shown in Fig. 6. The pole was not modeled aeroelastically because, as previously explained, this research is concerned with arm-pole relative displacements.

Tests were conducted in TTU's Boundary Layer Wind Tunnel which has a 1.8 m wide by 1.2 m high working section. The velocity scale was again 1.24:1. Each model was tested under different angles of attack for two different turbulence intensities: (1) nominally Exposure D, as specified by the ASCE (2005), and (2) low turbulence smooth flow. At the mast arm height, the first simulation had a turbulence intensity (TI) of about 16%, while the second had a TI of about 6%, as measured with a Turbulent Flow Series 100 Cobra Probe. Details of the simulation are presented in Cruzado (2007). The angle of attack convention used is shown in Fig. 1(b). This is the same that was used for the full-scale experiments (Cruzado 2007). Table 2 indicates the conditions of TI and angle of attack for which each model (with or without backplates) was tested.

For each of the different cases tested, data was collected at several wind speeds. For each data collection, a target wind speed was sought in the wind tunnel and, once obtained, data was recorded for one minute. At no point was the tip of the model restricted. Therefore, the tip of the model was free to vibrate when the target wind speed was being sought and data was not being recorded.

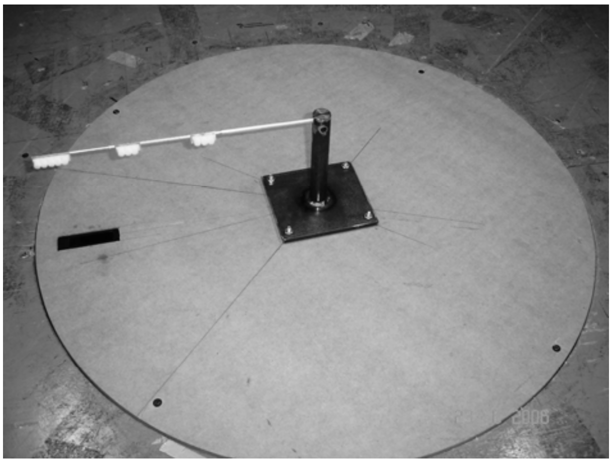

Fig. 6 Aeroelastic model of mast arm mounted in TTU wind tunnel

A Micro-Epsilon ILD-1401 laser displacement sensor with a resolution of 20 μm was used to measure cross-wind displacements of the tip of the model. The laser was placed beneath the turntable floor below the mast arm, so as not to interfere with the wind flow. The wind speed in the wind tunnel was measured at the height of the model's mast arm, by a Turbulent Flow Series 100 Cobra Probe placed 45 cm upstream of the model. Both probes were sampled at 1,000 Hz.

A pluck test was conducted to determine the fundamental frequency in the vertical direction and the damping ratio of the models. The results are presented in Table 3.

2.2.3 Results

For each angle of attack and wind speed tested in the wind tunnel, stationary data was recorded for one minute. For each test the average wind speed and the standard deviation of the vertical displacement were calculated and scaled to the full-scale. Using the cross-wind width *B* (58-cm and 37-cm in full-scale for the cases of with and without backplates, respectively), an average non-dimensional tip displacement d/B was calculated. Likewise, using the vertical fundamental frequency f_o = 1 Hz and the cross-wind width *B*, a reduced wind velocity of $U/f_o B$ was calculated. For each angle of attack tested, a plot was generated for the reduced wind velocity vs. the average non-dimensional tip displacement. Some of these plots are shown in the following figures, were

BP stands for backplates.

Fig. 7 shows the results obtained for the case of the models tested with an angle of attack of 90°. The figure shows that for all four test cases there is a spike in the vibration amplitude when the reduced wind speed is between 5 and 15. In the case of models with backplates, the spike is much larger than for the cases without backplates. These low-speed spikes represent a narrow band resonant response typical of vibrations caused by vortex shedding. This behavior was observed when the model with backplates was tested at angles of attack between 55° and 125° with

Table 2 Cases for which experiments were conducted

Angle of attack (degrees)	Exposure D (TI = 16%)		Smooth flow (TI = 6%)	
	With backplates	Without backplates	With backplates	Without backplates
0	X	X	X	
15			X	
25			X	
35	X		X	
45	X	X	X	
55	X		X	
65	X		X	
75	X		X	
85	X		X	
90	X	X	X	X
95	X		X	
105	X		X	
115	X		X	
125	X		X	
135	X	X	X	
145	X		X	
180	X	X	X	
225	X	X	X	
270	X	X	X	
315	X	X	X	

X = Experiment conducted for this case

Table 3 Vertical fundamental frequency (f_o) and damping ratio (ζ) of models

Model	f_o (Hz)	ζ (%)
With backplates	62	0.33
Without backplates	62	0.51

vibrations achieving peak amplitude when the reduced wind speed is around 8.5. The peak response was achieved for angle of attacks between 85° and 95°. Clearly, the wide range of reduced velocities for the large response represents phenomena beyond classical von Kármán vortex shedding. However, the fact that the peak responses are centered on a reduced velocity around 10 is indicative of a vortex shedding phenomenon.

Table 4 provides the maximum displacement values for the experiments conducted with 90° angle of attack. Clearly the response with backplates is much larger than those without backplates.

For the case of the model with backplates with an angle of attack of 55°, the maximum amplitude of vibration commences at reduced wind speeds exceeding 8, but extend over a much broader range of wind speeds as shown in Fig. 8.

For the case of the model with backplates under smooth flow, when the angle of attack was either 45° (Fig. 9) or 125° (Fig. 10) there were two spikes in the data instead of the typical single

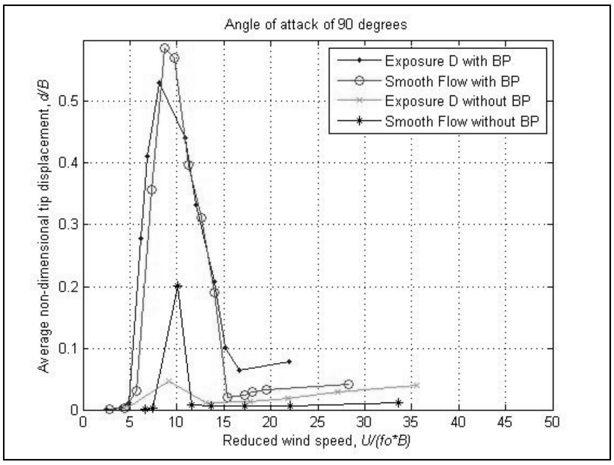

Fig. 7 Wind tunnel results for angle of attack of 90° for TTU wind tunnel tests

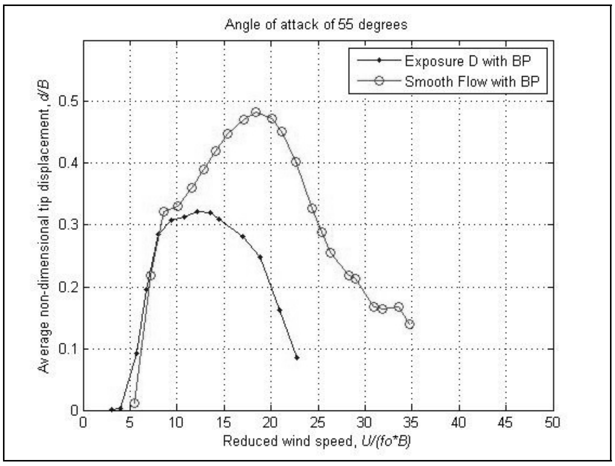

Fig. 8 Wind tunnel results for angle of attack of 55 degrees for TTU wind tunnel tests

Table 4 TTU full-scale equivalent results for 90° angle of attack

Flow	TI (%)	Max. average non-dimensional tip displacement	
		With backplates	Without backplates
Exposure D	16	0.53	0.047
Smooth	6	0.57	0.20

spike. In both cases, the first peak occurs at reduced wind speed range of about 8, while the second one occurs at a reduced wind speed range of approximately 25.

For the case of the model with backplates under smooth flow, when the angle of attack was 135° there was a spike in the data followed by an increase in the amplitude of the vibration with an increase in wind speed, as shown in Fig. 11. The increase in amplitude with an increase of speed suggests the galloping phenomenon.

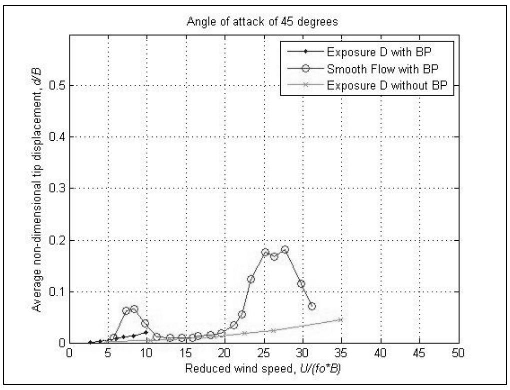

Fig. 9 Wind tunnel results for angle of attack of 45 degrees for TTU wind tunnel tests

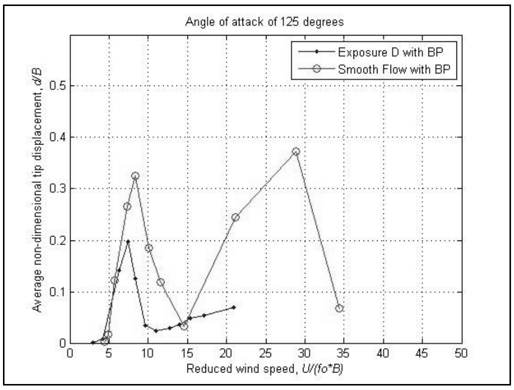

Fig. 10 Wind tunnel results for angle of attack of 125 degrees for TTU wind tunnel tests

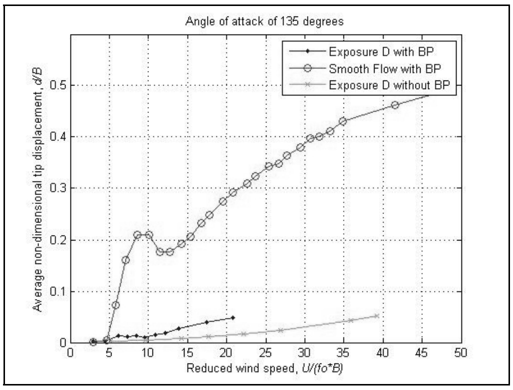

Fig. 11 Wind tunnel results for angle of attack of 135 degrees for TTU wind tunnel tests

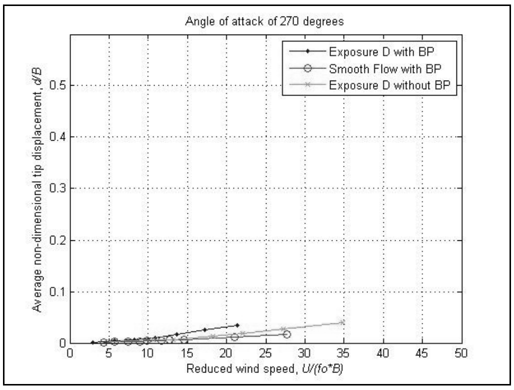

Fig. 12 Wind tunnel results for angle of attack of 270 degrees for TTU wind tunnel tests

Cases when the angle of attack was outside of the range of 45° to 135° did not exhibit large amplitude vibrations (an example of this is shown in Fig. 12). In many of these cases, data at wind speeds higher than those presented in the plots was not collected because horizontal (along-wind) displacements became too large, preventing the laser displacement sensor from recording accurate measurements. This was evidenced by the laser sensor recording vertical displacements of infinite value. Still, the models were visually inspected under higher wind speeds and no significant vertical vibrations were observed.

Fig. 13 was obtained by plotting the maximum value of the standard deviation of the displacement observed when the full-scale reduced wind speed was in the range of 0 to 15 for each angle of attack. The case of smooth flow without backplates is not included in the figure because,

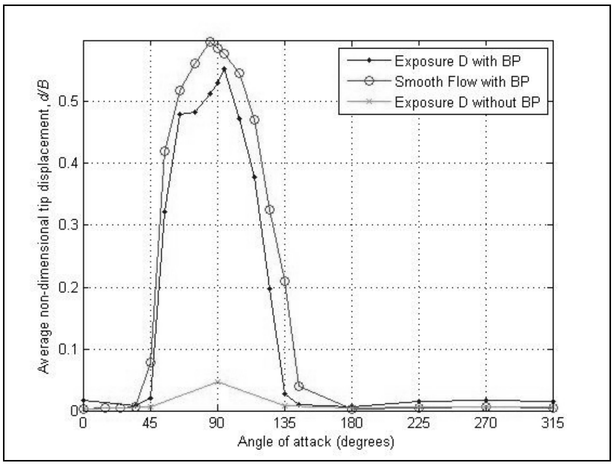

Fig. 13 Maximum amplitude of vibration observed for full-scale reduced wind speed in the 0 to 15 range for TTU wind tunnel tests

as indicated in Table 2, data was only collected for this case at an angle of attack of 90°. Three observations that can be made from Fig. 13 are:

1. Structures with backplates have larger vibrations than those without them.
2. Vibrations with large amplitude occur when the angle of attack is between 45° and 135°.
3. In the critical range of angle of attack of 45° to 135°, the magnitude of vibrations decreases as turbulence intensity increases.

The values plotted in Fig. 7 were used to evaluate the Strouhal number (*St*) for the different test cases, being the inverse of the reduced velocity at which the maximum average non-dimensional tip displacement occurs. The results are presented in Table 5. The values obtained for *St* are close to 0.12 computed for the full-scale data of March 29, 2005 (Cruzado 2007). The Strouhal Number for a flat plate perpendicular to the flow is ~0.15 (Blevins 1977; Hirsch and Bachmann 1995) while for flat plates with trailing features or T-shaped, *St* ranges from 0.11 to 0.14 (ASCE 1961) which are similar to the results found here.

Table 5 Calculation of Strouhal number (*St*)

Case	Maximum average non-dimensional tip displacement	Reduced velocity at which maximum response occurs	*St*
Exposure D with backplates	0.53	8.00	0.13
Smooth flow with backplates	0.57	9.62	0.10
Exposure D without backplates	0.047	9.15	0.11
Smooth flow without backplates	0.20	10.03	0.10

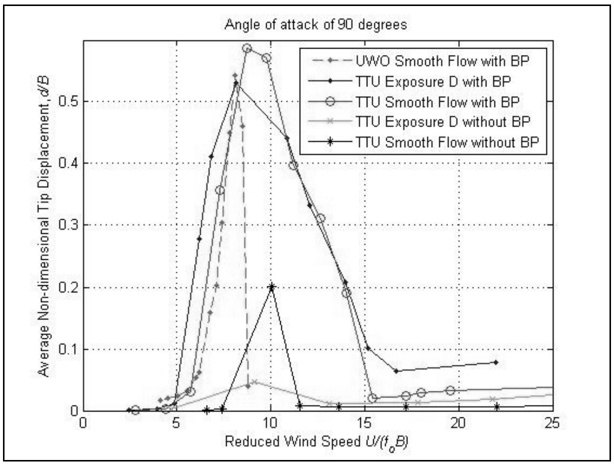

Fig. 14 Comparison of UWO and TTU test results for angle of attack of 90 degrees

3. Conclusions

Wind tunnel tests of a generic cantilever traffic signal structure in wind tunnels at the University of Western Ontario (UWO) and Texas Tech University (TTU) were conducted with identical models. The major difference between the two studies was that the mast arm model was orientated vertically at UWO, while at TTU was orientated horizontally. In Fig. 14, the results for the case of the wind approaching the signals from the back obtained at UWO (previously presented in Fig. 5), are compared with ones obtained in TTU for an angle of attack of 90 degrees (previously presented in Fig. 7). In the lowest turbulent flows similarities in response of the aeroelastic traffic signal model were observed, namely a narrow band resonant response at a reduced velocity range of 5 to 10.

The results of testing an aeroelastic model in two different wind tunnels indicate that vortex shedding can induce large amplitude vibrations of mast arms. Most of the time, vortex shedding was identified as the primary cause of these vibrations because of the characteristic specific speed range for large amplitude vibration. That the speed ranges at which the high amplitude vibrations occurred were not particularly narrow (especially in the TTU experiments) suggests that the vibrations are vortex-induced by a more complex phenomenon that goes beyond classic von Kármán vortex shedding. This and demands more extensive testing at larger length scales and a study examining interactions between mast arm attachments (signal heads) for varying angles of attack.

Structures that have signals with backplates can undergo much larger vibrations than structures that do not have backplates. Also, not unexpectedly, the amplitude of vibrations increases as the turbulence intensity decreases. For these vibrations to occur, the wind must be blowing towards the back of the signals, with an angle of attack in the range 45º to 135º and at full scale wind speeds in the range of 2 to 7 m/s.

The findings of these wind tunnel experiments agree with some of the findings initially reported by Pulipaka (1995), mainly that large-amplitude vibrations of mast arms are more prone to occur when the signals have backplates and when the wind blows from the back of the signals. On the other hand, galloping, which is generally considered to be the main cause of fatigue failure, was only observed in this study for an angle of attack of 135 degrees with the signals having backplates (Fig. 11). A typical galloping behavior would be to increase the magnitude of vibrations with an increase of wind speed, yet this was only observed for an angle of attack of 135^o under very smooth flow. This contradicts the notion that galloping is the main cause of fatigue failures of cantilever traffic signal structures. The experiments did reveal that there are complex interactions between angle of attack and response which is likely to be the case with vortices being shed from upwind backplates and interacting with downwind structures (visors) for particular oblique wind directions.

Acknowledgements

This work was funded by the Texas Department of Transportation under Project No. 04586 and by the National Science Foundation under Grant No. 0221688. The experiments were carried out while both H.J. Cruzado and C. Letchford were employed at the Wind Science and Engineering Center of Texas Tech University. G.A. Kopp gratefully acknowledges the support provided by the Canada Research Chairs Program.

References

AASHTO (2001), *Standard specifications for structural supports for highway signs, luminaires, and traffic signals*, 4th ed, Washington, DC, American Association of State Highway and Transportation Officials.

ASCE (1961), *Wind Forces on Structures*, Trans ASCE, 126 Part II, 1124.

Blevins, R. D. (1977), *Flow-induced vibration*, New York, Van Nostrand Reinhold Company.

Chen, G., Wu, J., Yu, J., Dharani, L.R. and Barker, M. (2001), "Fatigue assessment of traffic signal mast arms based on field test data under natural wind gusts", *Transport. Res. Record*, **1770**, 188-194.

Christenson, R.E. and Hoque, S. (2011), "Reducing fatigue in wind-excited traffic signal support structures using an innovative vibration absorber", In TRB 90th Annual Meeting Compendium of Papers DVD. Washington, DC, Transportation Research Board.

Cook, R.A., Bloomquist, D., Richard, D.S. and Kalajian, M.A. (2001), "Damping of cantilevered traffic signal structures", *J. Struct. Eng*., **127**(12), 1476-1483.

Cruzado, H.J. (2007), *Risk assessment model for wind-induced fatigue failure of cantilever traffic signal structures*, PhD dissertation, Texas Tech University.

Cruzado, H.J. and Letchford, C. (2013), "Full-scale experiments of cantilever traffic signal structures", *Wind Struct.* (submitted)

Dexter, R.J. and Ricker, M.J. (2002), *Fatigue-resistant design of cantilevered signal, sign, and light supports*, National Cooperative Highway Research Program Report 469, Washington, DC, National Cooperative Highway Research Program.

Gray, B., Wang, P., Hamilton, H.R. and Puckett, J.A. (1999), "Traffic signal structure research – Univ. of Wyoming", In Structural Engineering in the 21st Century, *Proceedings of the 1999 Structures Congress* held in New Orleans, Louisiana, April 18-19, (Ed., R. Avent and M. Alawady), 1107-1110, Reston, VA: American Society of Civil Engineers.

Hamilton III, H.R., Riggs, G.S. and Puckett, J.A. (2000), "Increased damping in cantilevered traffic signal structures", *J. Struct. Eng*. **126**(4), 530-537.

Hartnagel, B.A. and Barker, M.G. (1999), "Strain measurements of traffic signal mast arms" In Structural Engineering in the 21st Century, *Proceedings of the 1999 Structures Congress* held in New Orleans, Louisiana, April 18-19, 1999, edited by R. Avent and M. Alawady, 1111-1114. Reston, VA: American

Society of Civil Engineers.

Hirsch, G.H. and Bachmann, H.(1995), "Dynamic effects from wind. Appendix H of Vibration problems in structures: Practical guidelines", by Hugo Bachman *et al*. Basel, Switzerland, Birkhäuser.

Kaczinski, M.R., Dexter, R.J. and Van Dien, J.P. (1998), "*Fatigue-resistant design of cantilevered signal, sign, and light supports*", National Cooperative Highway Research Program Report 412, Washington, DC, National Academy Press.

McManus, P.S., Hamilton, H.R. and Puckett, J.A. (2003), "Damping in cantilevered traffic signal structures under forced vibration", *J. Struct. Eng*., **129**(3), 373-382.

Puckett, J.A., Erikson, R.G. and Peiffer, J.P. (2011), "Fatigue testing of stiffened traffic signal structures", *J. Struct. Eng*., **136**(10), 1205-1214.

Pulipaka, N. (1995), *Wind-induced vibrations of cantilevered traffic signal structures*, PhD dissertation, Texas Tech University.

Pulipaka, N., Sarkar, P.P. and McDonald, J.R. (1998), "On galloping vibration of traffic signal structures", *J. Wind Eng. Ind. Aerod*., **77 / 78** , 327-336.

Zuo, D. and Letchford, C.W. (2010), "Wind-induced vibration of a traffic-signal-support structure with cantilevered tapered circular mast arm", *Eng. Struct*., **32**, 3171-3179.

CC